NJC

Accepted Manuscript

This is an *Accepted Manuscript*, which has been through the Royal Society of Chemistry peer review process and has been accepted for publication.

Accepted Manuscripts are published online shortly after acceptance, before technical editing, formatting and proof reading. Using this free service, authors can make their results available to the community, in citable form, before we publish the edited article. We will replace this *Accepted Manuscript* with the edited and formatted *Advance Article* as soon as it is available.

You can find more information about *Accepted Manuscripts* in the **Information for Authors**.

Please note that technical editing may introduce minor changes to the text and/or graphics, which may alter content. The journal's standard **Terms & Conditions** and the **Ethical guidelines** still apply. In no event shall the Royal Society of Chemistry be held responsible for any errors or omissions in this *Accepted Manuscript* or any consequences arising from the use of any information it contains.

New Journal of Chemistry

ARTICLE

Manganese dioxide-vulcan carbon@silver nanocomposites for the applications of highly sensitive and selective hydrazine sensors

Kaliyamoorthy Justice Babu,[a] Awan Zahoor,[b] Kee Suk Nahm,*[b] Md. Abdul Aziz[c] Periasamy Vengadesh,[d] and Georgepeter Gnana kumar*[a]

Manganese dioxide (MnO_2) - vulcan carbon (VC) @ silver (Ag) (core@shell) nanocomposites were synthesized through a simple wet chemical method without using hazardous organic reagents, polymeric micelles, templates and catalysts. The synthesized MnO_2-VC@Ag exhibited a MnO_2-VC core and Ag shell, and the thickness of shell is found to be 23 nm. The obtained diffraction patterns confirmed that the prepared nanocomposite consists of tetragonal and face-centred cubic structures of MnO_2 and Ag nanostructures, respectively. The cyclic voltammetry and amperometric techniques were adopted to electrochemically characterize the MnO_2-VC@Ag nanospheres toward the hydrazine oxidation in phosphate buffer solution. Under the optimized conditions, the fabricated sensor exhibited good electrochemical performance toward hydrazine oxidation, offering broad linearity of 0.1 to 350 µM, with a relatively low detection limit of 100 nM and high sensitivity of 0.33 µAµM^{-1}cm^{-2}. In addition, the anti-interference property, good reproducibility, long term performance, good repeatability and real sample analysis were achieved for the constructed sensor, owing to the synergetic effects of Ag and MnO_2-VC nanostructures. The aforesaid attractive analytical performances and facile preparation of MnO_2-VC@Ag core-shell nanospheres provided new features of electrocatalytic activities and may hold good assurance for the design and development of effective hydrazine sensors.

1. Introduction

Hydrazine and its methyl derivatives are neurotoxin and produces mutagenic and carcinogenic effects with the low threshold limit value of 10 ppb, which damages the liver, kidneys, lungs, respiratory tract infection and long term effects on the central nervous system.[1,2] It has also been employed as a reactant in military fuel cells, corrosion inhibitor in boilers, rocket propellant, antioxidant, pesticide, photography chemicals, weapons for mass destruction, emulsifiers, dyes etc.,[3-5] Although hydrazine is widely used for the aforesaid applications, it is recognized as an environmental pollutant, owing to its high toxicity, which induces blood abnormalities, damages Deoxyribo Nucleic Acid (DNA), and deteriorates the nervous system.[5-7] The acute exposure to high content of hydrazine includes irritation of eyes, throat nose, dizziness, nausea, pulmonary edema, coma etc.,[1,8,9] Hence, it is essential to fabricate a sensitive, economically affordable and efficient analytical devices for the routine analysis of hydrazine in chemical, environmental and biological industries.[10] The electrochemical technique has been emerged as a preferential method for the detection of hydrazine, owing to their high sensitivity, excellent repeatability, excellent selectivity, low detection limit, long term stability and ease of miniaturization[11,12], which are superior over the potentiometry,[13] chemiluminescence,[14] chromatography,[15] and spectrophotometry[16] techniques. However, the high over-potential exhibited by the bare electrodes toward hydrazine oxidation urges its modification.[17,18] In the state of the art mediator-modified electrodes, organic electron mediators,[19] deoxyribonucleic acid (DNA),[20] ionic liquids[21] and inorganic metal complexes[22] have been widely exploited to decrease the over-potential of developed systems toward the hydrazine oxidation. However, the major problem encountered with the mediator-modified electrodes is their lack of stability, owing to the leach out of mediator from the electrode surface. Recently, nanostructures modified electrodes have been widely used for the development of electrochemical sensors, which exhibits several advantages such as high mass transport, low detection limit, lower solution resistance, better signal-to-noise ratio, high sensitivity and excellent selectivity.[23-27] On the basis of above, keen research efforts have been devoted toward the manganese dioxide (MnO_2) nanostructures on the account of its low cost, high energy density, environmental benign characteristics and high abundance.[28,29] However, bare MnO_2 nanostructures are not effectual enough to provide the excellent oxidation kinetics toward hydrazine molecules due to its loose tunnel structure, lower electrical conductivity, agglomeration in aqueous solution and dissolution issues, which urges the utilization of an active carbon support.[30] Vulcan carbon

[a] Department of Physical Chemistry, School of Chemistry, Madurai Kamaraj University, Madurai-625-021, Tamil Nadu, India.
[b] School of Chemical Engineering and Department of Energy Storage and Conversion Engineering, Chonbuk National University, Jeonju-561-756, Republic of Korea.
[c] Center of Excellence in Nanotechnology, King Fahd University of Petroleum and Minerals Dhahran, 31261, Saudi Arabia.
[d] Low Dimensional Materials Research Centre (LDMRC), Department of Physics, Faculty of Science, University of Malaya, 50603 Kuala Lumpur, Malaysia.

(VC) is considered as an unique active carbon support, owing to its high electrical conductivity, high stability in both acidic and basic media and flexibility in the textural and surface chemical properties.[31,32] In addition, it also exhibits the specific advantages including low cost, ease of fabrication, wide potential window, tunability, miniaturization and surface renewability.[31-33]

Recently, core@shell nanostructures have received immense attention, owing to the excellent stabilization of nanostructures, high adsorption of an analyte and prevention of leaching and agglomeration of nanomaterials.[34] The core@shell nanomaterials exhibit specifically exposed active sites, which may be beneficial for probing the analyte during the electrocatalysis process. Furthermore, the strong interaction exerted between core and shell nanostructures provide the excellent physical or chemical contacts, which may maintain the structural stability and offer novel electrochemical properties.[34,35] In this research effort $MnO_2VC@Ag$ core@shell nanostructures have been developed on the basis of excellent new chemical activities, owing to the tuned electron transfer between MnO_2-VC and Ag and other integrated properties of individual components. The present work is aimed to identify the influence of chemical and morphological features of prepared nanostructures toward the hydrazine electrooxidation under various electrochemical regimes and conditions.

2. Experimental methods

2.1. Materials

Potassium permanganate ($KMnO_4$, AR, Merk, ≥98.5%), manganese (II) sulfate trihydrate ($MnSO_4 \cdot 3H_2O$, AR, Merk, ≥99.5%) silver nitrate ($AgNO_3$, Sigma-Aldrich, 99.99%), ascorbic acid (AA, AR, Sigma-Aldrich, ≥99.5%), dopamine (DA, AR, Sigma-Aldrich, ≥99%), citric acid (CA, AR, Merk, ≥99.5%), glucose (GLU, GC, Sigma-Aldrich, ≥99.5%), hydrazine sulphate ($N_2H_4SO_4$, Sigma-Aldrich, ≥99.0%), magnesium sulphate ($MgSO_4$, AR, Merk, ≥99.5%), potassium chloride (KCl, AR, Merk, ≥99.5%), uric acid (UA, HPLC, Sigma-Aldrich, ≥99%), sodium chloride (NaCl, AR, Merk, ≥99.5%), copper chloride ($CuCl_2$, AR, Merk, ≥99.0%), potassium ferrous cyanide ($K_4[Fe(CN)_6]$, ACS, Sigma-Aldrich, ≥99.0%) and Manganese chloride($MnCl_2$, AR, Merk, ≥99.5%) were purchased and employed without any further purification.

2.2. Synthesis of MnO_2-VC

100 mg VC was added in 0.1 M $KMnO_4$ solution and magnetically stirred for 1 h and the mixture was refluxed at 83 °C for 30 min under atmospheric conditions.[23] The precipitate was collected *via* centrifugation and washed with de-ionized water and dried at 120 °C overnight for further use.

2.3. Synthesis of MnO_2-VC@Ag

For the preparation of MnO_2-VC@Ag (1:1), 0.1 M $AgNO_3$ was dissolved in 0.1 M $KMnO_4$ and magnetically stirred for 1 h. 100 mg VC was added in the suspension and the mixture was refluxed at 83 °C for 30 min under atmospheric conditions. The precipitate was collected *via* centrifugation and washed with de-ionized water and dried at 120 °C for 12 h. The similar procedure was adopted for the preparation of 1:2, 1:5 and 1:7 ratios of MnO_2-VC:Ag composites by fixing the aforesaid concentration of $KMnO_4$-VC and comparatively increasing the amount of Ag content. On the basis of the ratio between Ag and MnO_2-VC, the prepared samples were denoted as

MnO_2-VC@Ag(1:1), MnO_2-VC@Ag(1:2), MnO_2-VC@Ag(1:5) and MnO_2-VC@Ag(1:7).

2.4. Modification of electrodes

The glassy carbon electrode (GCE, diameter of 3 mm and area 0.07 cm^2) was carefully polished according to the procedure described elsewhere.[23-25] The as-prepared nanostructure was dispersed in ethanol (2 mg ml^{-1}) and ultrasonicated for 30 min and the electrode surface was modified through the 6 µl suspension and dried under normal atmospheric conditions. To fix the electrocatalyst, 0.5 % Nafion was drop cast over the modified electrode and dried at room temperature. The MnO_2-VC, MnO_2-VC@Ag(1:1), MnO_2-VC@Ag(1:2), MnO_2-VC@Ag(1:5) and MnO_2-VC@Ag(1:7) modified electrodes were denoted as MnO_2-VC/GCE, MnO_2-VC@Ag(1:1)/GCE, MnO_2-VC@Ag(1:2)/GCE, MnO_2-VC@Ag(1:5)/GCE, and MnO_2-VC@Ag(1:7)/GCE, respectively.

2.5. Characterizations

The X-ray diffraction (XRD) patterns of prepared nanostructures were obtained from Rigaku D/max-2500 equipped with Cu Kα radiation (I = 1.54178 A°) with the Bragg angle ranging from 5 to 85 °. The morphology, shape and size of the nanostructures were obtained by using FESEM -JEOL JEM-2010 and transmission electron microscopy (TEM) (Hitachi-H-7650). The elemental composition and distributions were performed by using a Hitachi-H-7650 SEM equipped with the energy dispersive spectrometer (EDX) analysis.

2.6. Electrochemical characterizations

The electrochemical measurements were performed by using a one compartment three-electrode cell with bare or modified GCE as a working electrode and Pt wire and Ag/AgCl as the auxiliary and reference electrode, respectively. The cyclic voltammograms (CV) of studied electrodes were monitored by using a computer-controlled CHI-650E electrochemical workstation. The CVs of bare or modified electrodes were evaluated in 0.1 M PBS (pH-7.2) at a scan rate of 100 mVs^{-1} under the absence and presence of 5 mM hydrazine, and the amperometric experiments were carried out in 0.1 M PBS (pH-7.2) solution with the successive injection of hydrazine at an applied potential of 0.45 V *vs.* Ag/AgCl.

3. Results and discussion

3.1. Crystalline structure of the synthesized catalysts

The homogeneous dispersion of MnO_2 over the active VC support was achieved through the direct reduction of Mn(VII) into Mn(IV) by the sacrificial oxidation of carbon support. The MnO_2 nanostructures served as domains for the deposition of Ag nanoshell formation and the direct reduction of Ag$^+$ ions into Ag^0 achieved *via* MnO_2-VC spheres leads to the formation of MnO_2-VC@Ag core-shell nanostructures. The structure, morphological features and elemental composition of prepared nanomaterials were evaluated and its influences toward the electrochemical oxidation of hydrazine were studied in detail. The intimate contact exerted among the different components of developed nanostructure may facilitate the efficient electron conduction and the metallic active sites are expected to electrochemically oxidize the hydrazine.
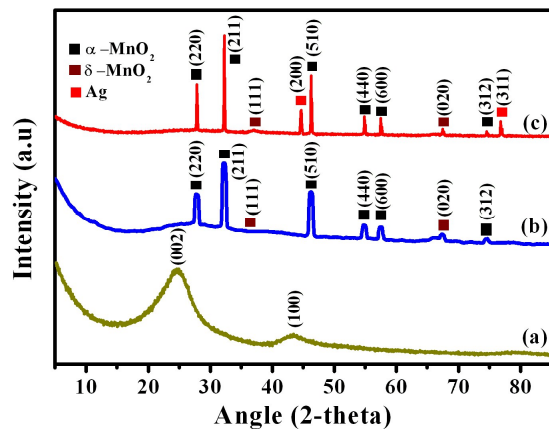
Please do not adjust margins

Fig. 1 XRD patterns of (a) VC, (b) MnO$_2$-VC and (c) MnO$_2$-VC@Ag(1:5).

Fig. 1 depicts the diffraction patterns of prepared nanostructures and VC exhibited the broad peaks at 24.6 and 43.4 ^{o} (Fig. 1a), corresponding to the (002) and (100) reflection planes, respectively, of the graphitic structure of activated carbon particles. MnO$_2$/VC exhibited the significant diffraction peaks at 27.83, 32.36, 46.24, 54.90, 57.58 and 74.54 ^{o} (Fig. 1b), representing the (220), (211), (510), (440) (600) and (312) reflection planes of α–MnO$_2$ (JCPDS No. 44–0141, tetragonal, I4/m), respectively.[23] Furthermore, the characteristic reflection planes of (111) and (020) were also found for the prepared MnO$_2$-VC at 36.92 and 67.64 ^{o}, respectively, representing the δ phase of MnO$_2$ (JCPDS No. 80–1098, monoclinic, C2/m)[23] (Fig. 1b), specifying that the prepared MnO$_2$ nanostructure is in transition state from δ-MnO$_2$ to α-MnO$_2$. MnO$_2$-VC@Ag(1:5) exhibited the aforementioned significant diffraction planes of MnO$_2$ along with the characteristic (200) and (311) reflection planes (Fig. 1c) of the face-centred cubic structures of Ag,[25] which confirmed the composite formation. The high intensities of characteristic Ag and MnO$_2$ diffraction peaks reduced the visibility of VC diffraction peaks in MnO$_2$-VC@Ag(1:5) composite.

3.2. Morphology and elemental composition of synthesized catalysts

The morphological features of prepared nanostructures were analyzed by using FE-SEM and the obtained micrographs are given in Fig.2. MnO$_2$-VC nanostructures exhibited the homogeneously distributed spherical nanoparticles with the average particle size of 60 nm (Fig. 2a). Although MnO$_2$-VC@Ag nanocomposites exhibited the spherical morphology, the regular building blocks with fused architectures with an enlarged diameter were observed for the composite, which is purely attributed to the anchoring of Ag nanoparticles in the MnO$_2$ lattices. The presence of fused structure in the product is ascribed to the vacancy flux resulting from the diffusivity differences at inorganic interfaces. It is also observed that a gradual increment in the diameter was observed for the prepared nanostructures with an increase in the Ag content and MnO$_2$-VC@Ag(1:1) (Fig. 2b), MnO$_2$-VC@Ag(1:2) (Fig. 2c) and MnO$_2$-VC@Ag(1:5) (Fig. 2d) exhibited the average particle size of 68, 74 and 87 nm, respectively. It is also evidenced that the composite formation of Ag with MnO$_2$-VC has not altered the spherical morphology and narrow size distribution of MnO$_2$-VC.
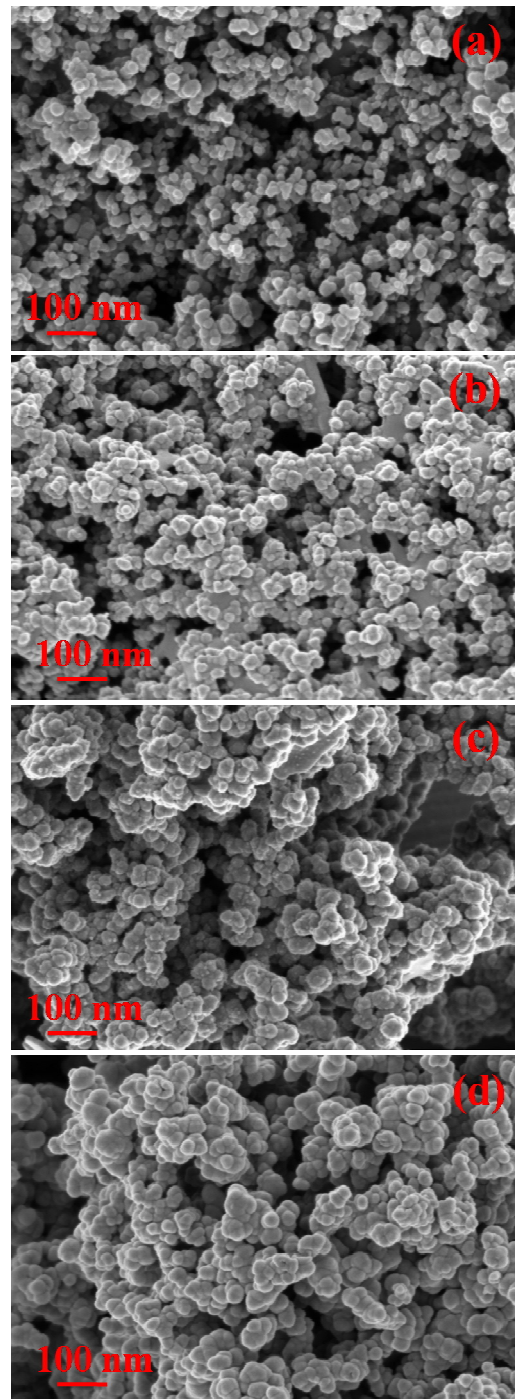

Fig. 2 FE-SEM Images of (a) MnO$_2$-VC (b) MnO$_2$-VC@Ag(1:1) (c) MnO$_2$-VC@Ag(1:2) and (d) MnO$_2$-VC@Ag(1:5).

The EDX analysis (Fig. 3) was performed to evaluate the composite formation by monitoring the presence of carbon (C), oxygen (O), Ag and Mn elements. The EDX pattern of MnO$_2$-VC confirmed the presence of C, O and Mn elements (Fig. 3a). In addition with the above elements, MnO$_2$-VC@Ag (Fig. 3b) exhibited the Ag element that ensured the composite formation of Ag with
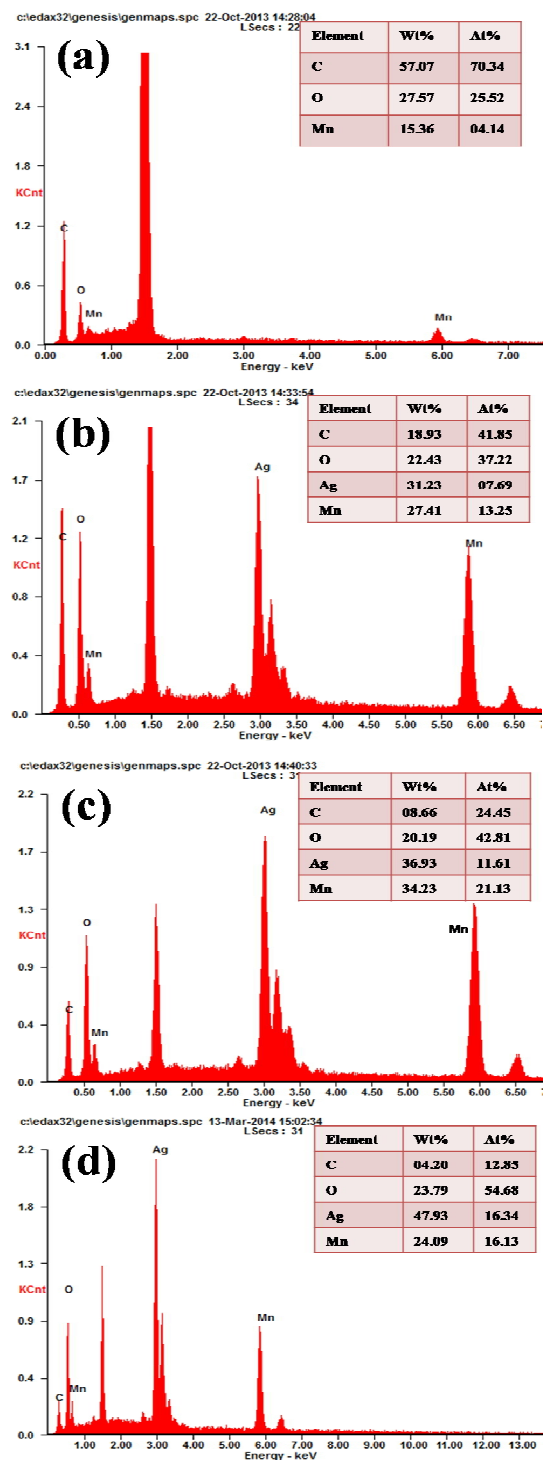
Element	Wt%	At%
C	57.07	70.34
O	27.57	25.52
Mn	15.36	04.14

Element	Wt%	At%
C	18.93	41.85
O	22.43	37.22
Ag	31.23	07.69
Mn	27.41	13.25

Element	Wt%	At%
C	08.66	24.45
O	20.19	42.81
Ag	36.93	11.61
Mn	34.23	21.13

Element	Wt%	At%
C	04.20	12.85
O	23.79	54.68
Ag	47.93	16.34
Mn	24.09	16.13

Fig. 3 EDX images of (a) MnO_2-VC (b) MnO_2-VC@Ag(1:1) (c) MnO_2-VC@Ag(1:2) and (d) MnO_2-VC@Ag(1:5).
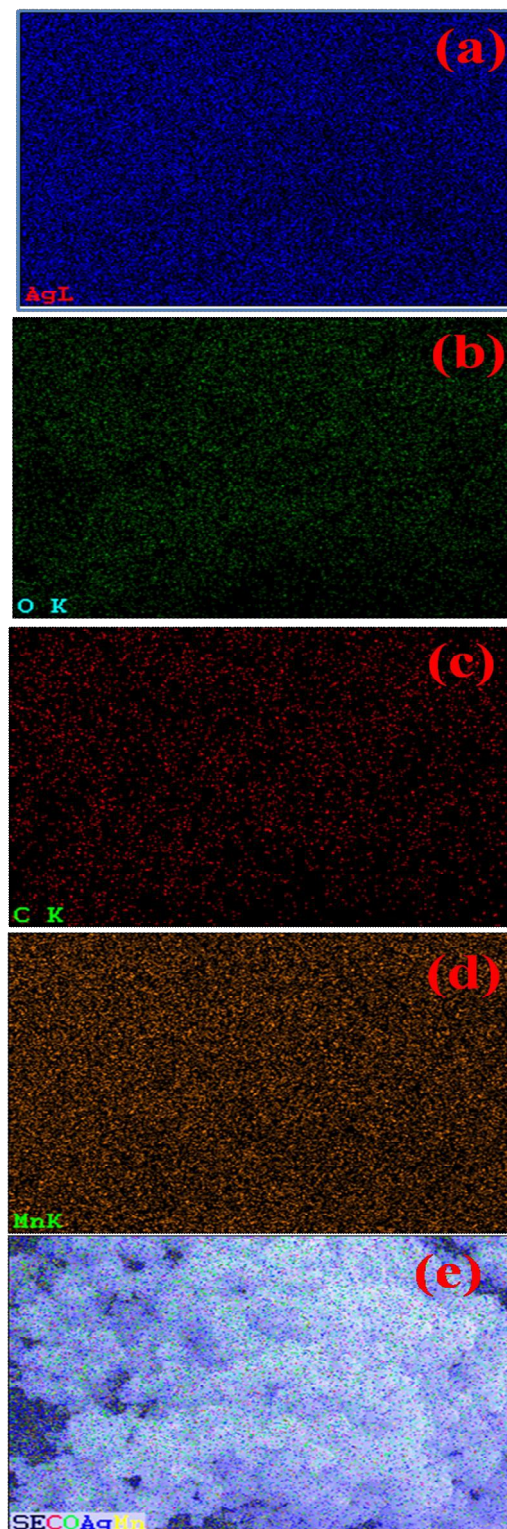
Fig. 4 (a) Ag, (b) O, (c) C and (d) Mn elemental mapping of MnO_2-VC@Ag(1:5) and (e) its corresponding SEM image.
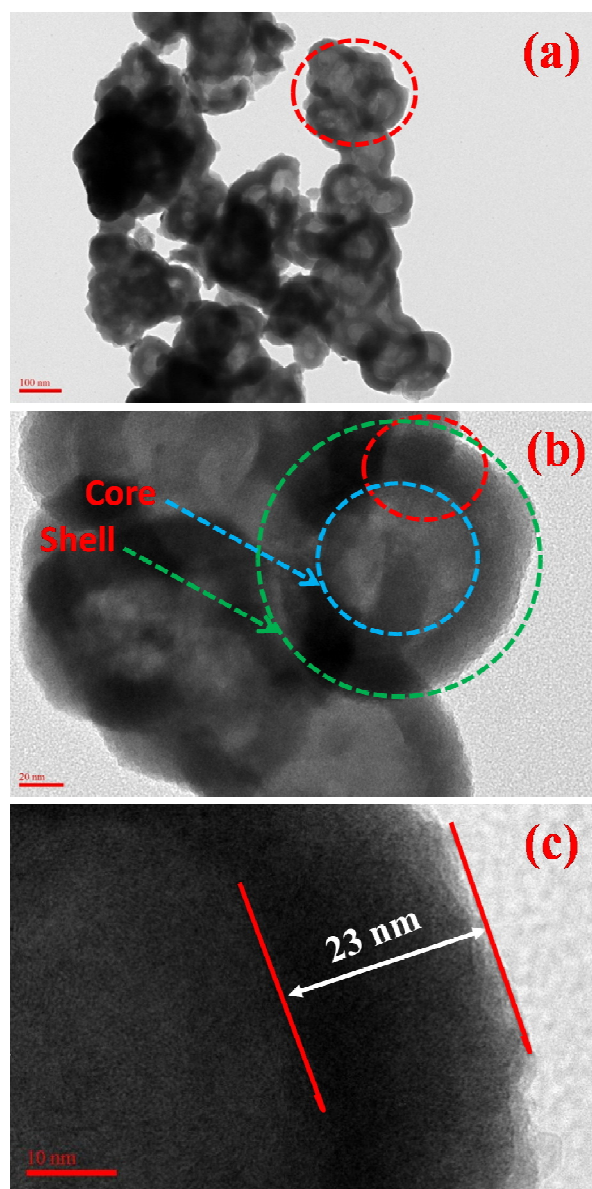
Fig. 5 TEM images of (a-b) MnO$_2$-VC@Ag(1:5) (core@shell particle has been outlined by the dashed circles) and (c) corresponding HRTEM image.

MnO$_2$-VC. Furthermore, an increase in the Ag content in MnO$_2$-VC was clearly observed from the increased Ag wt.% elemental composition (Fig. 3 b-d). The significant EDX peak observed at 1.5 keV for all of the prepared samples is attributed to the 'Al' element that arises from the aluminium foil utilized for the deposition of prepared nanostructures.

The distribution of elements present in the prepared MnO$_2$-VC@Ag (1:5) composite is convoluted from the elemental mapping (Fig. 4 a-d) and the mapped red, green, blue and yellow regions correspond to C, O, Ag and Mn elements respectively, indicating a homogeneous distribution of Ag, MnO$_2$ and VC throughout the core-shell nanospheres.

From Fig. 5 a-c, it is clear that the light-color core made up of MnO$_2$-VC is surrounded by the dark-color Ag shell, specifying the core@shell structure of a prepared MnO$_2$-VC@Ag(1:5) nanocomposite. The sacrificial oxidizing agent VC effectively reduced the Mn(VII) into Mn(IV) and generated an uniform thin layer of MnO$_2$ over its surface. The direct reduction of Ag$^+$ ions into Ag^0 achieved *via* MnO$_2$-VC lead to the Ag shell formation over the MnO$_2$-VC nanospheres. The average diameter of MnO$_2$-VC@Ag(1:5) composite is found to be 87 nm and the thickness of Ag shell is found to be 23 nm as evidenced from the high resolution TEM image (Fig. 5c), which is expected to facilitate the electrocatalytic activity of prepared composite.

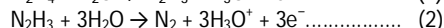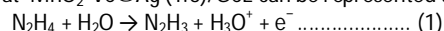### 3.3. Electrochemical behaviours of the studied electrodes

The background electrochemical properties of bare GCE, MnO$_2$-VC/GCE, MnO$_2$-VC@Ag(1:1)/GCE, MnO$_2$-VC@Ag(1:2)/GCE and MnO$_2$-VC@Ag(1:5)/GCE were studied by using cyclic voltammetry in 0.1 M PBS (pH-7.2) at a scan rate of 100 mVs^{-1} (Fig. 6a). The bare GCE has not exhibited any electrochemical redox peak at the potential window of - 0.2 to + 1.0 V. MnO$_2$-VC/GCE exhibited a pair of redox peaks, in which the anodic peak potential (E_{pa}) and the cathodic peak potential (E_{pc}) are located at + 0.48 and + 0.21 V *vs.* Ag/AgCl, respectively, which are assigned to the redox behaviour of MnO$_2$ species.[36] On the other side, MnO$_2$-VC@Ag(1:1)/GCE, MnO$_2$-VC@Ag(1:2)/GCE and MnO$_2$-VC@Ag(1:5)/GCE exhibited E_{pa} at 0.42 V *vs.* Ag/AgCl and E_{pc} at 0.01 V *vs.* Ag/AgCl, corresponding to the formation of Ag$_2$O and reduction of Ag$_2$O to Ag, respectively.[12,26] An increase in the Ag content on MnO$_2$-VC nanospheres gradually increased the peak currents, owing to the enhanced metallic active sites.

3.4. Electrocatalytic activities of studied electrodes toward hydrazine oxidation

In order to evaluate the electrocatalytic properties of bare and prepared nanostructures modified GCEs, the cyclic voltammograms were recorded in PBS under the presence of 5 mM hydrazine. The CVs recorded for bare GCE, MnO$_2$-VC/GCE, MnO$_2$-VC@Ag(1:1)/GCE, MnO$_2$-VC@Ag(1:2)/GCE, MnO$_2$-VC@Ag(1:5)/GCE and MnO$_2$-VC@Ag(1:7)/GCE in 0.1 M PBS (pH-7.2) at a scan rate of 100 mVs^{-1} are provided in Fig. 6b. The bare GCE exhibited a weak electrooxidation current toward hydrazine at 0.8 V *vs.* Ag/AgCl. On the other side, MnO$_2$/VC/GCE exhibited an increased oxidation current (Ipa) of 11.0 µA toward hydrazine oxidation, which is ascribed to the prompt catalytic activity of MnO$_2$ nanoparticles. Initially, hydrazine was effectively adsorbed over the active sites of MnO$_2$-VC surfaces and the generated Mn(IV) species effectively electrooxidzed the analyte hydrazine. The uniform and efficient distribution of VC and MnO$_2$ catalysts improved the covalent coupling between metal oxide and nanocarbon materials.[32] The integration of MnO$_2$ and VC facilitated the formation of electrically conducting network and provided a number of electrocatalytic sites, facilitating the charge transfer during the electrooxidation of hydrazine at the MnO$_2$ surfaces. Furthermore, the obviously enhanced anodic electrocatalytic currents were observed at fabricated MnO$_2$-VC@Ag/GCEs (Fig. 6b). MnO$_2$-VC@Ag/GCEs exhibited the oxidation and reduction peaks in the range of 0.54 to 0.67 and 0.17 to 0.27 V *vs.* Ag/AgCl, respectively (Fig. 6b). The observed reduction peak corresponds to the reduction of Ag$_2$O into Ag. The uniform core-shell nanosphere morphology coupled with

uniform distribution of carbon support provided the faster electronic transport and facile the electrocatalytic activity toward electroxidation of hydrazine. MnO_2-VC@Ag composite exhibited the high electrical conductivity, extended number of electrocatalytic

active sites and easier mass transport for the analyte diffusion. The core-shell formation of MnO_2 with the transition metal Ag lowered the activation potential and high d-band centers of composite facilitated the binding of an analyte Moreover, the core-shell structure maximized the interfacial surface area and strengthened the electron transfer between the individual components through surface bonds. The extended number of exposed active sites with dangling bonds on the surface of nanomaterials efficiently increased the interfacial contact with the analyte.[37,38] In addition, other unique properties of nanostructured materials including high surface to volume ratio, lattice distortion, electronic state density and charge transfer distribution were also beneficial for the superior catalytic activity of MnO_2-VC@Ag toward hydrazine oxidation.[39] The electrochemical oxidation mechanism of hydrazine is purely dependent upon the electrolyte solution and nature of the electrodes. Under the 0.1 M PBS (pH-7.2), hydrazine mostly presents in the unprotonated form (pKa = 7.9) and the trace level of protonated form exists in the oxidized hydrazine.[7] The electrochemical oxidation of unprotonated form of hydrazine achieved at MnO_2-VC@Ag (1:5)/GCE can be represented as follows:

$$N_2H_4 + H_2O \rightarrow N_2H_3 + H_3O^+ + e^- \text{.................... (1)}$$
$$N_2H_3 + 3H_2O \rightarrow N_2 + 3H_3O^+ + 3e^- \text{................. (2)}$$

The electrochemical oxidation of hydrazine involved one electron transfer process (rate determination step) and proceeded by the three electron transfer (speed reaction) process, leading to the formation of nitrogen (N_2) as a final product. The overall hydrazine oxidation reaction occurred at MnO_2-VC@Ag (1:5)/GCE is expressed as:

$$N_2H_4 + 4H_2O \rightarrow N_2 + 4H_3O^+ + 4e^- \text{.................. (3)}$$
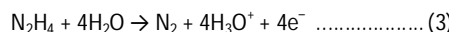
Furthermore, the electrooxidation of hydrazine at MnO_2-VC@Ag (1:5)/GCE is schematically illustrated in Fig. 6c.
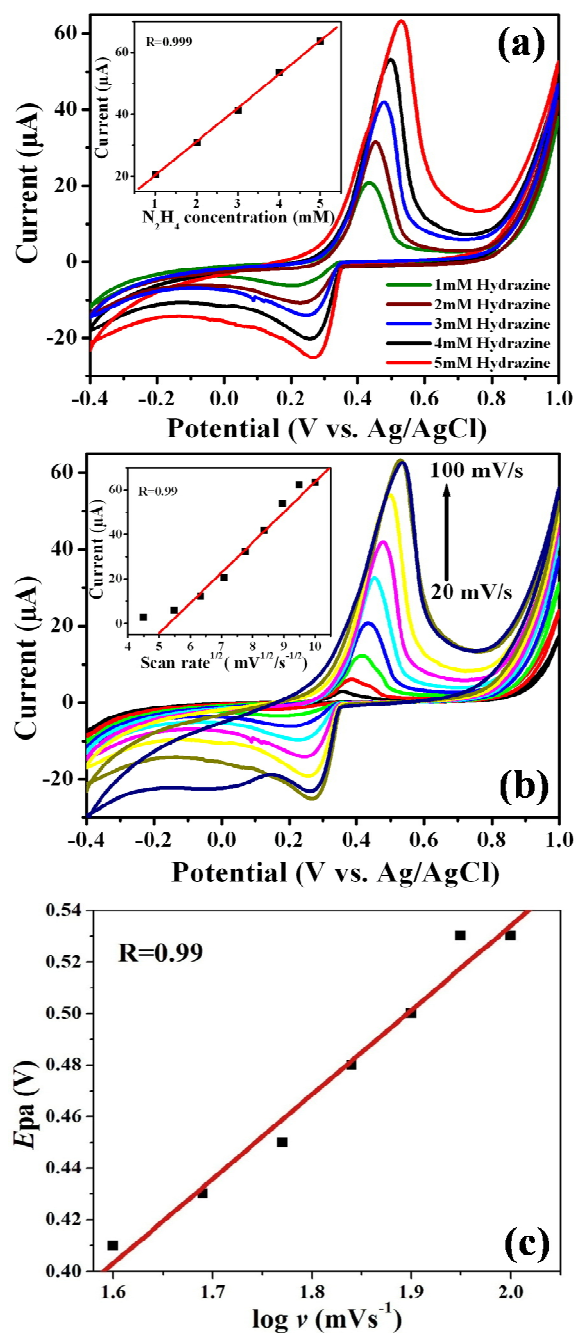
MnO_2-VC@Ag(1:1)/GCE, MnO_2-VC@Ag(1:2)/GCE, MnO_2-VC@Ag(1:5)/GCE and MnO_2-VC@Ag(1:7)/GCE exhibited the Ipa of 15.3, 19.6, 63.6 and 45.4 µA, respectively, toward hydrazine electrooxidation. Among the studied MnO_2-VC@Ag/GCEs, MnO_2-VC@Ag(1:5)/GCE exhibited a significantly improved I_{pa}, which is 4.0 and 3.5 fold higher than that of MnO_2-VC@Ag(1:1)/GCE and MnO_2-VC@Ag(1:2)/GCE. The enhanced electrocatalytic performance of MnO_2-VC@Ag(1:7)/GCE is attributed to the optimum thickness of (23 nm) of Ag nanoshell and well interconnected MnO_2-VC core that efficiently supplied the number of surface-active (i.e interfacial surface between Ag and MnO_2) sites for the adsorption of reactants and reduced the resistance to efficiently diffuse the analyte.[33] Further increasing the Ag content beyond (1:5) in MnO_2-VC@Ag, the hydrazine oxidation response was decreased. The decrement in the electrooxidation process at MnO_2-VC@Ag(1:7)/GCE, is attributed to the high loading of Ag, which blocked the exposed MnO_2 active surfaces with an analyte.

The dependence of electrochemical oxidation CVs on the hydrazine concentration is depicted in Fig. 7a. With an increase in the hydrazine concentration (1 - 5 mM) in the supporting electrolyte, the I_{pa} was increased with the positively shifted E_{pa} values. The obtained results indicated that the reaction involved mass transport and oxidation is purely dependent upon the hydrazine concentration at a sufficient potential, which is ideal for the quantitative analysis.

Fig. 7b depicts the CV curves of MnO_2-VC@Ag(1:5)/GCE in 0.1 M PBS (pH-7.2) containing 5 mM hydrazine as a function of scan rate ranging from 20-100 mVs^{-1}. It is found that I_{pa} of MnO_2-VC@Ag(1:5)/GCE is linearly increased with an increase in the square root of scan rate ranging from 20-100 mVs^{-1} with the high correlation coefficient (R) of 0.990, indicating that the involved
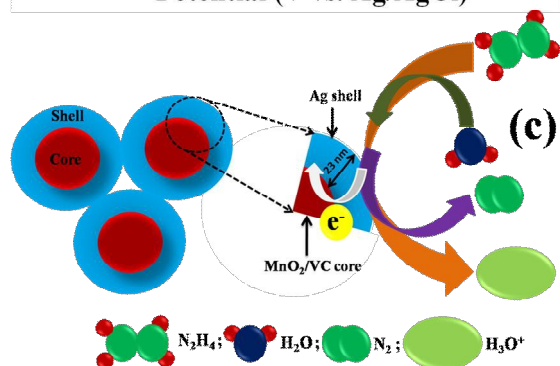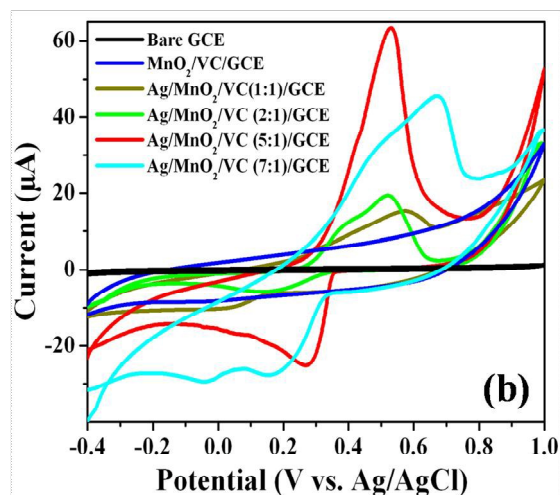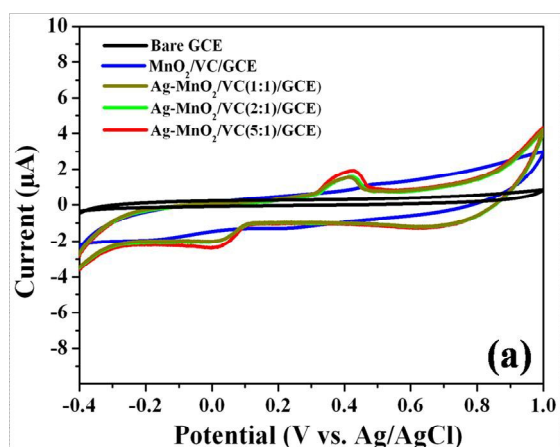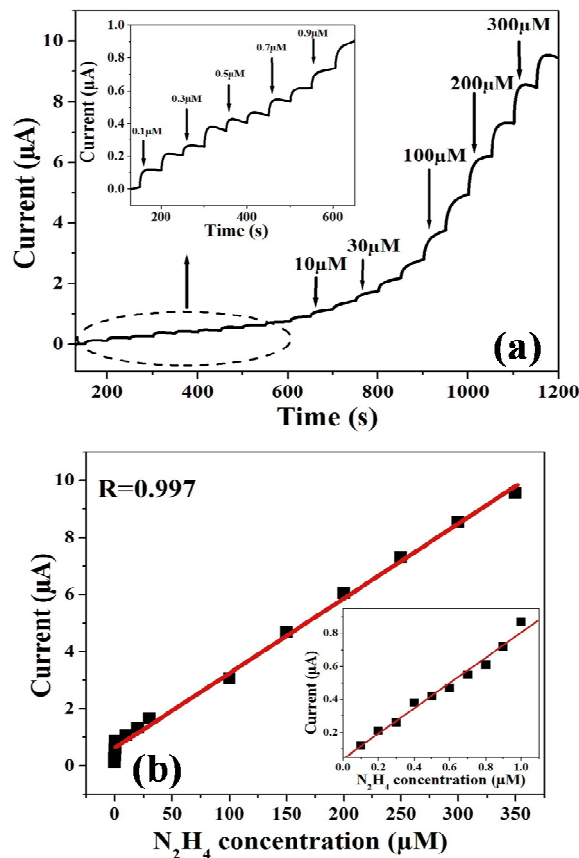
Fig. 6 CVs of studied at bare or modified GCEs obtained under the (a) absence and (b) presence of 5 mM hydrazine in 0.1 M PBS (pH-7.2) at a scan rate of 100 mVs^{-1}and (c) plausible reaction mechanism involved in the hydrazine electrooxidation.

Fig. 8 (a) Amperometric responses observed at MnO_2-VC@Ag(1:5)/GCE in 0.1 M PBS (pH-7.2) during the successive addition of different concentration of hydrazine at an applied potential of 0.45 V *vs.* Ag/AgCl (inset: amperometric responses of 0.1 -1.0 µM) and (b) plot of concentration dependence signal *vs.* hydrazine concentration (inset : plot of concentration dependence signal *vs.* hydrazine concentration (0.1 -1.0 µM).

Fig. 7 CVs obtained at MnO_2-VC@Ag(1:5)/GCE (a) as a function of different concentration of hydrazine at a scan rate of 100 mVs^{-1} (inset : corresponding calibration plot I_{pa} *vs.* concentration of hydrazine), (b) as a function of scan rates ranging from 20-100 mVs^{-1} in the presence of 5 mM hydrazine (inset : corresponding calibration plot I_{pa} *vs.* Square root of scan rates) and (c) the corresponding plot of E_{pa} *vs.* log *v*.

In addition, a linear relationship between E_p and log *v* has also been deduced (Fig. 7c), suggesting that a kinetic limitation was involved in the reaction between redox sites of MnO_2-VC@Ag(1:5) and hydrazine. For an irreversible electron-transfer electrode process, the slope of the plot of E_{pa} *vs.* log *v* for the anodic reaction is 2.303 RT/(1−α)nF[40] as per the Laviron theory, where α and n stands for the charge transfer co-efficient and number of electrons involved in the rate determining step, respectively, and the charge transfer co-efficient (α) is found to be 0.81.

3.5. Amperometric current - time responses at MnO_2-VC@Ag(1:5)/GCE toward the electrooxidation of hydrazine

Based on the voltammetric results, amperometric *i-t* experiment was carried out to estimate the detection limit and sensitivity of MnO_2-VC@Ag(1:5)/GCE toward hydrazine electrooxidation and the amperometric current responses were recorded at an applied potential of 0.45 V *vs.* Ag/AgCl in 0.1M PBS (pH-7.2). After the successive addition of hydrazine (as marked in Fig. 8a) into a stirred

reaction is a diffusion-controlled electrochemical process at MnO_2-VC@Ag(1:5)/GCE (inset: Fig. 7b).

Table 1 Comparison of the electroanalytical performances of different electrochemical hydrazine sensors using different modified electrodes.

| Electrode materials	Response (s)	Linear range (μM)	LOD[a] (μM)	Sensitivity (μA/μM·cm²)	Reference
MnO$_2$/MWCNT[b]/GCE[c]	5	0.5-1000	0.2	-	41
MnHCF[d]/GWCE[e]	<4	33.3–8180	6.65	0.0475	42
OAP[f]/GCE[c]	-	2.0-20.0	0.05	0.016 μA/μM	43
HMWCNT[g]/GCE[c]	<2	2.0–122.8	0.68	0.0208	44
Cu–Pd/GCE[c]	<4	2–100	0.27	0.21 μA/μM	45
Graphene nanoflakes/GCE[c]	<3	0.5–7	0.3	0.028	46
Pd/MWNT[b]	<10	2.5–700	1.0	-	47
CM[h]/MWCNT[b]/GCE[c]	<3	2.0–44.0	1.4	22.9 nA/μM	48
PANI[i]/Ag/GCE[c]	-	20–100	-	-	49
PVP[j]/AgNCs/GCE[c]	<2	5.0-460	1.1	-	26
Mn$_2$O$_3$ NFs[k]/GCE[c]	5	up to 644	0.3	474 mA/mM cm²	50
Graphene/GCE[c]	<3	3.0-300	1.0	-	51
Pd/BDD[l]	-	10-102	1.8	4.7 A/M cm²	52
CuS/rGO[m]/GCE[c]	-	1-1000	0.3	7.9642 μA/mM	53
CuO/Si nanowire	<3	1-5000	0.25	-	54
Ag/MnO$_2$/VC/GCE[c]	5	0.1-350	0.1	0.33	This work

Limit of detection[a]; Multi walled carbon nanotubes[b]; Glassy carbon electrode[c]; manganese hexacyanoferrate[d]; Graphite–wax composite electrode[e]; o-aminophenol[f]; Hematoxylin multi-wall carbon nanotubes[g]; Curcumin[h]; Polyaniline[i]; Poly(vinylpyrrolidone)[j]; nanofibers[k]; boron-doped diamond[l]; reduced graphene oxide[m];

PBS solution, the peak current was constantly increased with an increase in the hydrazine concentration (Fig. 8a). 94 % of steady state current was reached within 5 s, revealing that the fabricated sensor exhibited fast response toward hydrazine electrooxidation, owing to the enhanced electrical conductivity afforded by the MnO$_2$/VC with the decoration of Ag nanoparticles. The obtained amperometric currents were plotted against hydrazine concentration (Fig. 8b) and MnO$_2$-VC@Ag(1:5)/GCE exhibited the wider linear range ranging from 0.1 - 350 μM with the high correlation co-efficient R= 0.997 (n=19), the detection limit is estimated to be 100 nM at 3sb/S; where sb-standard deviation of blank signal and S- sensitivity.[23] The sensitivity was calculated from the slope of linear range plot and is observed to be 0.33 μAμM^{-1}cm^{-2} for MnO$_2$-VC@Ag(1:5)/GCE. The obtained hydrazine sensor performances are suitably compared with the previously reported hydrazine sensors (Table 1) and it is clear that the properties such as wide linear range, detection limit, sensitivity and response time obtained at Ag/MnO$_2$/VC(1:5)/GCE are either superior or comparable over the reported literatures.[41-54]

3.6. Effect of interfering species, stability reproducibility and real sample analysis of MnO$_2$-VC@Ag(1:5)/GCE

It is well-known that DA, AA, GLU and CA are the common interfering species in physiological samples. In addition, high

amount of metal ions such as Fe^{2+}, Cu^{2+}, Mg^{2+}, Na$^+$, Mn^{2+} and Cl$^-$ usually exist in water samples. Hence, the interference tests were conducted by measuring the current changes caused by the addition of 3 mM DA, AA, GLU, CA and 80 mM of Fe^{2+}, Cu^{2+},
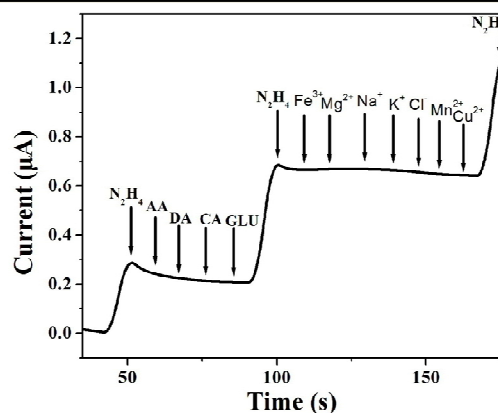
Fig. 9 Interfering responses over hydrazine signal at MnO$_2$-VC@Ag (1:5)/GCE in 0.1 M PBS (pH-7.2) at 0.45 V *vs.* Ag/AgCl.

ARTICLE

Mg^{2+}, Na^{+}, Mn^{2+} and Cl^{-}. The amperometric responses were obtained at MnO$_2$-VC@Ag(1:5)/GCE by the successive injection of 0.3 µM hydrazine and interfering species, the increased current response was observed with 0.8 µM hydrazine (Fig. 9). On the other side, no obvious current response was observed with the high concentration of DA, AA, GLU, CA, Fe^{2+}, Cu^{2+}, Mg^{2+}, Na^{+}, Mn^{2+} and Cl^{-}. These results demonstrated that the fabricated sensor exhibited excellent selectivity toward hydrazine and completely avoided the interfering effects from the other electroactive species.

To investigate the reproducibility of proposed method, six MnO$_2$-VC@Ag(1:5)/GCEs were fabricated under the similar conditions and CV experiments were conducted under the presence of 5 mM hydrazine. A relative standard deviation (RSD) of 3.8 % was obtained for a series of MnO$_2$-VC@Ag(1:5)/GCE, resulting the good reproducibility of prepared sensors. The operational stability of fabricated sensor was also monitored through the electrooxidation of hydrazine for every 3 days for 24 consecutive days and MnO$_2$-VC@Ag(1:5)/GCE was stored at room temperature, when not in use. It was found that the MnO$_2$-VC@Ag(1:5)/GCE retained about 92.5% of its original response to hydrazine oxidation after one month of storage, indicating the good stability of fabricated systems. The strong interaction exerted between the core and shell nanostructures provided the unique physical and chemical contacts and maintained the structural stability, which improved the electrochemical durability performances.

The quantitative detection of hydrazine in drinking water samples has received keen interest, owing to the importance of controlling water based diseases. In order to evaluate the validity of fabricated sensors in the detection of hydrazine in real sample analysis, the amperometric current responses of MnO$_2$-VC@Ag(1:5)/GCE were monitored by spiking the known concentrations of hydrazine in two drinking water samples at an applied potential of 0.45 V *vs.* Ag/AgCl. The recovery obtained for the fabricated system is in the range of 98-106 % associated with a 2.9-3.8 % relative standard deviation (Table 2), validating the practical applications of fabricated sensors.

Table 2 Detection of hydrazine in drinking water samples using MnO$_2$-VC@Ag(1:5)/GCE.

Sample Used	Hydrazine added (µM)	Hydrazine found (µM)	R.S.D.[a] (%)	Recovery (%)
1	10	10.2	3.6	102
	20	19.6	3.2	98
	30	31.0	3.8	103
2	10	10.6	3.8	106
	20	20.8	3.4	104
	30	29.4	2.9	98

[a] Relative standard deviation.

4. Conclusion

MnO$_2$-VC@Ag core@shell nanospheres were prepared by a facile, efficient, and economical route and exploited as the electrooxidation probes of hydrazine. The obtained morphological

characterizations ensured the core-shell formation of MnO$_2$-VC@Ag nanostructures and the diffraction patterns elucidated the tetragonal and fcc structures of MnO$_2$ and Ag, nanostructures, respectively. The electrocatalytic activity of MnO$_2$-VC@Ag core-shell nanospheres toward hydrazine oxidation was analyzed by using CV technique without using any redox mediator. From the amperometric i-t experiments, it is clear that the proposed sensor exhibited the low detection limit, high sensitivity and good selectivity. Furthermore, the sensor demonstrated practical applicability in real samples, good reproducibility and high stability over 24 days. The facile preparation protocols and good sensor performances potentially offer the promising opportunities for the chemical and biosensor applications.

Notes and references

1 S. D. Zelnick, D. R. Mattieand and P. C. Stepaniak, *Aviat. Space Environ. Med.,* 2003, **74,** 1285.
2 S. Garrod, M. E. Bollard, A. W. Nicholls, S. C. Connor, J. Connelly, J. K. Nicholson, and E. Holmes, *Chem. Res. Toxicol.,* 2005, **18,** 115.
3 J. W. Mo, B. Ogorevc, X. Zhang and B. Pihlar, *Electroanalysis,* 2000, **12,** 48.
4 S. J. R. Prabakar and S. S. Narayanan, *J. Electroanal. Chem.,* 2008, **617,** 111.
5 C. B. McAuley, C. E. Banks, A. O. Simm, T. G. J. Jones, and Compton, R. G. *Analyst,* 2006, **131,** 106.
6 A. A. Ibrahim, G. N. Dar, S. A. Zaidi, A. Umar, M. Abaker, H. Bouzid, and S. Baskoutas, *Talanta,* 2012, **93,** 257.
7 C. Karuppiah, S. Palanisamy, S. M. Chen, S. K. Ramaraj, and P. Periakaruppan, *Electrochim. Acta,* 2014, **139,** 157.
8 C. A. Reilly, and S. D. Aust, *Chem. Res. Toxicol.,* 1997, **10,** 328.
9 G. Choudhary and H. Hansen, *Chemosphere,* 1998, **37,** 801.
10 R. Sivasubramanian and M. V. Sangaranarayanan, *Sens. Actuators, B,* 2015, **213,** 92.
11 K. Ramachandran, K. J. Babu, G. G. Kumar, A. R. Kim and D. J. Yoo, *Sci. Adv. Mater.,* 2015, **7,** 329.
12 A. Safavi, and M. Tohidi, *Anal. Methods,* 2012, **4,** 2233.
13 E. A. Malaki, and M. A. Koupparis, *Talanta,* 1989, **36,** 431.
14 A. Safavi, and M. R. Baezzat, *Anal. Chim. Acta,* 1998, **358,** 121.
15 M. Mori, K. Tanaka, Q. Xu, M. Ikedo, H. Taoda and W. Hu, *J. Chromatogr. A,* 2004, **1039,** 135.
16 M. George, K. S. Nagaraja, and N. Balasubramanian, *Talanta,* 2008, **75,** 27.
17 Y. Ding, Y. Wang, L. Zhang, H. Zhang, C. M. Li, and Y. Lei, *Nanoscale,* 2011, **3,** 1149.
18 M. M. Ardakani, Z. Taleat, H. Beitollahi and H. Naeimi, *Nanoscale,* 2011, **3,** 1683.
19 L. Niu, T. You, J. Y. Gui, E. Wang and S. J. Dong, *J. Electroanal. Chem.,* 1998, **448,** 79.
20 G. Chang, Y. Luo, W. Lu, J. Hu, F. Liao and X. Sun, *Thin Solid Films,* 2011, **519,** 6130.
21 N. Maleki, F. Safavi, E. Farjami and F. Tajabadi, *Anal. Chim. Acta,*

2008, **611,** 151.

22 S. S. Narayanan, and F. A. Scholz, *Electroanalysis,* 1999, **11,** 465.

23 K. J. Babu, A. Zahoor, K. S. Nahm, R. Ramachandran, M. A. J. Rajan, and G. G. Kumar, *J. Nanopart. Res.,* 2014, **16,** 2250.

24 J. Salamon, Y. Sathishkumar, K. Ramachandran, Y. S. Lee, D. J. Yoo, A. R. Kim and G. G. Kumar, *Biosens. Bioelectron.,* 2015, **64,** 269.

25 G. G. Kumar, K. J. Babu, K. S. Nahm and Y. J. Hwang, *RSC Adv.,* 2014, **4,** 7944.

26 Y. Wang, X. Yang, J. Bai, X. Jiang and G. Fan, *Biosens. Bioelectron.,* 2013, **43,** 180.

27 J. Zhang, W. Gao, M. Dou, F. Wang, J. Liu, Z. Li, and J. Ji, *Analyst,* 2015, **140,** 1686.

28 Z. Chen, Z. Jiao, D. Pan, Z. Li, M. Wu, C. H. Shek, C. M. L. Wu and J. K. L. Lai, *Chem. Rev.,* 2012, **112,** 3833.

29 W. Chen, R. B. Rakhi, Q. Wang, M. N. Hedhili, and H. N. Alshareef, *Adv. Funct. Mater.,* 2014, **24,** 3130.

30 G. G. Kumar, A. Zahoor, K. S. Nahm, and J. S. Xavier, *Biosens. Bioelectron.,* 2014, **53,** 528.

31 Z. Yang, J. Ren, Z. Zhang, X. Chen, G. Guan, L. Qiu, Y. Zhang and H. Peng, *Chem. Rev.,* 2015, **115,** 5159.

32 R. M. A. Hameed, *Biosens. Bioelectron.,* 2013, **47,** 248.

33 T. Soboleva, K. Malek, Z. Xie, T. Navessin and Holdcroft, *ACS Appl. Mater. Interfaces,* 2011, **3,** 1827.

34 G. W. Yang, G. Y. Gao, C. Wang, C. L. Xu, and H. L. Li, *Carbon,* 2008, **46,** 747.

35 G. Maduraiveeran, and R. Ramaraj, *Anal. Chem.,* 2009, **81,** 7552.

36 J. Lei, X. Lu, W. Wang, X. Bian, Y. Xue, C. Wang and L. Li, *RSC Adv.,* 2012, **2,** 2541.

37 M. Cirillo, T. Aubert, R. Gomes, R. V. Deun, P. Emplit, A. Biermann, H. Lange, C. Thomsen, E. Brainis, and Z. Hens, *Chem. Mater.,* 2014, **26,** 1154.

38 K. Maeda, K. Teramura, D. Lu, N. Saito, Y. Inoue and K. Domen, *Angew. Chem.,* 2006, **118,** 7970.

39 W. K. Bae, J. Kwak, J. W. Park, K. Char, C. Lee and S. Lee, *Adv. Mater.,* 2009, **21,** 1690.

40 E. Laviron, *J. Electroanal. Chem.,* 1979, **101,** 19.

41 M. Wang, C. Wang, G. Wang, W. Zhang and F. Bin, *Electroanalysis,* 2010, **22,** 1123.

42 D. Jayasri and S. S. Narayanan, *J. Hazard. Mater.,* 2007, 144, 348.

43 H. M. Nassef, A. E. Radi and C. K O'Sullivan, *J. Electroanal. Chem.,* 2006, **592,** 139.

44 H. R. Zare and N. Nasirizadeh, *Electrochim. Acta,* 2007, **52,** 4153.

45 C. C. Yang, A. S. Kumar, M. C. Kuo, S. H. Chien, and J. M Zen, *Anal. Chim. Acta,* 2005, **554,** 66.

46 S. Mutyala and J. Mathiyarasu, *Sens. Actuators, B,* 2015, **210,** 692.

47 J. Zhao, M. Zhu, M. Zheng, Y. Tang, Y. Chen and T. Lu, *Electrochim. Acta,* 2011, **56,** 4930.

48 L. Zheng and J. F. Song, *Sens. Actuators, B,* 2009, **135,** 650.

49 P. Paulraj, N. Janaki, S. Sandhya and K. Pandian, *Colloid. Surf. A,* 2011, **377,** 28.

50 Y. Ding, C. Hou, B. Li and Y. Lei *Electroanalysis,* 2011, **23,** 1245.

51 C. Wang, L. Zhang, Z. Guo, J. Xu, H. Wang, K. Zhai and X. Zhuo, *Microchim. Acta,* 2010, **169,** 1.

52 C. B. McAuley, C. E. Banks, A. O. Simm, G. J. J. Timothy and G. C. Richard, *Analyst,* 2006, **131,** 106.

53 Y. J. Yang, W. Li, and X. Wu, *Electrochim. Acta,* 2014, **123,** 260.

54 Z. Guo, M. L. Seol, M. S. Kim, J. H. Ahn, Y. K. Choi, J. H. Liu, X. J. Huang, *Nanoscale,* 2012, **4,** 7525.

Active carbon supported MnO_2@Ag nanocomposite was developed for the highly sensitive and selective electrochemical detection of hydrazine

Shell

Core

Ag shell

23 nm

e^-

MnO_2-VC core

N_2H_4 ; H_2O ; N_2 ; H_3O^+